Oral presentation | Incompressible/compressible/hypersonic flow
Incompressible/compressible/hypersonic flow-I
Wed. Jul 17, 2024 2:00 PM - 4:00 PM Room D

[8-D-02] Evaluation of Active Drag in Freestyle Swimming using the Immersed Boundary Surface Method

*Alexander Haskins[1], Alex Lennon[1], Adrian Murphy[1], Dominic Chandar[1] （1. Queen's University Belfast）

Keywords: Immersed boundary methods, Active drag, Swimming, Unsteady, RANS

**Twelfth International Conference on
Computational Fluid Dynamics (ICCFD12),
Kobe, Japan, July 14-19, 2024**

Evaluation of Active Drag in Freestyle Swimming using an Immersed Boundary Surface Method

A. Haskins*, C. McCabe**, R. Keating**, A. Lennon*, A. Murphy* and D. Chandar*
Corresponding author: ahaskins02@qub.ac.uk
* School of Mechanical and Aerospace Engineering, Queen's University Belfast, Belfast, UK
** School of Sport, Ulster University, Belfast, UK

Abstract: Computational and experimental evaluations of active drag experienced during fully submerged human swimming are compared and discussed. Experimentally (using a load cell, commercial resistance trainer, and method from existing literature), the active drag of a swimmer swimming solely underwater was measured. The measured active drag profile was reasonable compared to existing literature, with peak drag values estimated between 200-250 N. Computationally, the foam-extend fork of OpenFOAM was used in all calculations. Active drag was predicted using complex geometry validation via passive drag simulations, quasi-steady cases, and moving body cases. Variations in swimming technique were also investigated using quasi-steady means. Passive drag was estimated using the immersed boundary surface method in the open-source Foam-Extend, with solutions provided using the simpleFoam and pimpleDyMIbFoam solvers. Results, approximately equal to 105 N at 2.00 ms, were higher than typical estimates from literature but compared more favourably to cases with geometry in a more similar position. Quasi-steady approaches and variable velocity approaches predicted reasonable estimates for the active drag profile, with slightly slightly lower predictions compared to the experimental results. Moving body simulations struggled to predict reasonable estimates of active drag. Analysis of potential sources of error indicated it is likely that results could be improved with more accurate swimming animations and a smoother geometry.

Keywords: OpenFOAM, Active Drag, Immersed Boundary Method, Quasi-steady.

1 Introduction

Active drag is the resistive force that acts on a swimmer when swimming through the water and is constantly changing during a stroke cycle [1] [2]. A stroke cycle in swimming is a movement that returns to its beginning and repeats itself in the same sequence. A thorough understanding of an individual's active drag profile is necessary, especially at the elite level (where winning margins are frequently small), in order to optimise technique, minimise active drag, and maximise forward velocity. Active drag is difficult to measure directly, largely due to complex fluid motion and accessibility limitations, meaning researchers use indirect methods to estimate values of active drag. One such method that could prove insightful is through the use of computational fluid dynamics (CFD). To overcome common difficulties encountered when performing CFD on moving geometries, such as a swimmer, this study aimed to investigate the ability of the immersed boundary method(IBM) to estimate active drag during swimming.

2 Literature Review

2.1 Freestyle Technique

The current study will primarily focus on Freestyle, one of the four main disciplines in swimming. At the top level of competition, the Freestyle events range from 50 m (approx. 20 s of swimming) to 1500 m (approx. 14 min 30 s of swimming) with technique changes clearly visible between sprint-based events and distance-based events. The current accepted general Freestyle technique is outlined below.

Freestyle is swum on the front with the head planted firmly in the water. Key characteristics include the alternating arm motion for each stroke and alternating leg motion for each kick. The propulsion phase begins with the catch. The catch is made with an outstretched arm placed to the front of the body. A common feature of the stroke is a high elbow, allowing for a good purchase in the water during the catch and ensuring efficient propulsion through the water as the arm moves down by the swimmer's side towards the end of the propulsion phase. The arm is recovered above the surface of the water before returning to the initial starting position to begin the catching process again. The catch and recovery are combined with a rolling body motion, used to make the stroke more efficient by increasing stroke length. Although the swimmer is on their front, a large portion of Freestyle is swum when the chest is not in the horizontal plane, due to the aforementioned rolling motion [3].

The breath is taken when the body is rotated to the side, with one arm outstretched in front at the beginning of the catch and one arm at the end of the pull through phase to ensure as much speed as possible is retained during the breath. The breathing motion depends on the swimmer, with some choosing to alternate breathing to each side every three or five strokes and some choosing to breathe to one side every two or four strokes. Breathing frequency tends to increase with fatigue[3].

The kick is a simple up and down motion with an outstretched ankle acting as a fin. The rate of kick also depends on swimmer preference, with some choosing to do a two-beat kick (two kicks for every stroke), widely used in distance swimming, and some choosing to do a six-beat kick (six kicks for every stroke), widely used in shorter sprint events[3].

2.2 Active drag experimental methods

Active drag is a culmination of frictional drag, pressure drag, and wave drag, but separating these values can prove complex experimentally. To date, there have been a number of experimental attempts to measure active drag and a handful of computational attempts. Typical experimental methods tend to assume a constant value of active drag across the stroke cycle, including the Measurement of active drag (M.A.D.) system developed by Hollander and the Velocity Perturbation Method (VPM) [4] [5]. Across a freestyle stroke cycle, the velocity and wetted surface area are constantly changing, meaning it is unlikely that drag will be constant across a full stroke cycle.

Haskins et al [6] developed a new method for experimentally predicting the active drag of a swimmer across a full stroke cycle, instead of assuming an average active drag for the full stroke. This was done by using a multiple tension force collection method, involving two experiments: one fully tethered and one semi tethered. Another experimental method that does function to show the changing drag profile is the assisted towing method (ATM), used by Mason and Formosa [7] [8]. The assisted towing method allows the athlete to swim with normal technique, whilst being towed at a slightly higher swimming velocity. The method is very similar to the VPM, although the athlete is towed towards the equipment. These methods, in theory, would allow the investigation of how technique impacts active drag as the full drag profile is found.

Although many of these methods provide reasonable estimations of what the value of active drag will be during Freestyle, many limitations arise. All these methods are invasive and must have some impact on a swimmer's technique and many of these methods assume a constant power across experiments or the stroke. As a result of this, it is likely that a non-invasive method could provide a better approximation of active drag.

2.3 Active drag computational methods

Computationally, Matt Keys[9] is one of the few researchers that have been able to run full body multi-phase simulations of freestyle across a full stroke cycle. Keys was concerned with maximising propulsion and minimising drag, recommending keeping feet submerged at all times and maximising acceleration at the beginning of an arm stroke, amongst other things. Although not stated how long these simulations took, assuming standard re-meshing is required at each time step, they can be assumed to have taken considerable time [9]. Beyond Keys, most active drag simulations are only concerned with flutter kick or butterfly kick. Von Loebekke et al.[10] performed some immersed boundary simulations of butterfly kick, but focussed on vortex production rather than active drag. Von Loebekke also did not provide a timescale for the simulations but it can be assumed, using a ghost cell immersed boundary method, time savings were made when compared to standard remeshing procedures [10].

Some success in computationally predicting the impact on net forces by stroke rate across a stroke cycle have been made using smoothed-particle hydrodynamcis (SPH) by Cohen and Mason [11]. The net force of the profile appears to be reasonable, especially when compared to the computational profile of Keys and other experimental data, such as the 1080 Sprint raw data collected by Haskins et al.[6] and the ATM results collected by Formosa and Mason [7] [8] . There is no indication of the time requirements in using SPH but it is assumed to be more computationally intensive than typical CFD methods.

Currently the computational resources required to run standard CFD and SPH cases are large, meaning CFD and SPH are less frequently used in order to investigate how a swimmer's active drag changes with technique. Regardless of this, CFD could provide an accurate approximation to how drag changes across a stroke cycle, due to the non invasive nature of the simulations, unlike the existing experimental active drag methods.

2.4 Problem Statement

The main problem that must be addressed in current CFD of swimming involves reducing the computational resources required in order to run these complex simulations, whilst maintaining sufficient accuracy to enable results to inform decisions about a swimmer's technique. The immersed boundary method could provide a computationally less intensive method to investigate active drag. The main aim of this paper was thus to investigate the capabilities in using the immersed boundary surface method in OpenFOAM[12] to predict drag around complex moving body swimming simulations. This problem will be answered using the following methods:

- Active drag experimental validation
- Complex geometry IBM - unsteady passive drag cases
- Quasi-steady IBM - basic geometry and active drag cases

2.5 Theory and Governing Equations

2.5.1 CFD

The following simulations are incompressible, governed by the continuity and momentum equations which have been included below in Equations 1 and 2 [13].

$$\nabla \cdot \mathbf{u} = 0 \tag{1}$$

$$\frac{\partial \mathbf{u}}{\partial t} + \nabla \cdot (\mathbf{u}\mathbf{u}) = -\frac{1}{\rho}\nabla p + \nabla \cdot (\nu \nabla \mathbf{u}) + S \tag{2}$$

where $\mathbf{u}$ is the velocity vector, p is the pressure, μ is the kinematic viscosity, and S is a general source term for additional forcing terms, which in this case is not required. The solutions to these governing equations are approximated using a finite-volume method (FVM), where the computational domain is divided into volumetric cells and the governing equations are solved using appropriate numerical schemes. The version of OpenFOAM used for solving all problems was Foam-extend-5.0, due to its immersed boundary method capabilities. Within this paper, there are single-phase steady, unsteady, and moving body problems that have been solved using simpleFoam,and pimpleDyMIbFoam [13].

2.5.2 Turbulence

A number of the following simulations are characterised by a high Reynolds number. Because of this, turbulence models must be introduced to account for some of the turbulence that is prevalent in these simulations. Throughout these simulations, the Reynolds-averaged Navier-Stokes (RANS) equations are solved, as opposed to the standard momentum equation. The RANS equations are a result of the Reynolds decomposition, were velocity is divided into a mean and fluctuating component. The RANS equations are included below [13]:

$$\frac{\partial U}{\partial t} + \nabla \cdot (U\mathbf{U}) = -\frac{1}{\rho}\frac{\partial P}{\partial x} + \nabla \cdot (\nu \nabla U) - \nabla \cdot (\overline{u'\mathbf{u}'}) \tag{3}$$

$$\frac{\partial V}{\partial t} + \nabla \cdot (V\mathbf{U}) = -\frac{1}{\rho}\frac{\partial P}{\partial y} + \nabla \cdot (\nu \nabla V) - \nabla \cdot (\overline{v'\mathbf{u}'}) \tag{4}$$

$$\frac{\partial W}{\partial t} + \nabla \cdot (W\mathbf{U}) = -\frac{1}{\rho}\frac{\partial P}{\partial z} + \nabla \cdot (\nu \nabla W) - \nabla \cdot (\overline{w'\mathbf{u}'}) \tag{5}$$

where $\mathbf{U}$ is the mean velocity vector, **u'** is the fluctuating velocity vector, U, V, and W are mean velocity components and u', v', and w' are fluctuating velocity components. During the simplification of the time-averaged convection term, a new term with fluctuating velocities appears, known as the Reynolds stress term. Because of this newly introduced Reynolds stress term, the RANS equations must be closed using turbulence models, in this case the two equation k-ϵ model. The Boussinesq hypothesis states that the Reynolds stresses are proportional to the mean deformation rates and can be described for incompressible flow as follows [13]:

$$-\rho\overline{\mathbf{u}' \otimes \mathbf{u}'} = -\mu_t[\nabla U + \nabla(U)^t] - \frac{2}{3}\rho k I \tag{6}$$

where is μ_t the eddy viscosity and k is the turbulent energy per unit mass [Eqn 7] [13].

$$k = \frac{1}{2}(\overline{(u')^2} + \overline{(v')^2} + \overline{(w')^2}) \tag{7}$$

2.5.3 k-ϵ turbulence model

The turbulent kinetic energy, k, and the viscous dissipation rate, ϵ, are used to define the velocity and length scales of the large scale turbulence as shown below [13]:

$$v = k^{\frac{1}{2}} \tag{8}$$

$$l = \frac{k^{\frac{3}{2}}}{\epsilon} \tag{9}$$

The eddy viscosity is then described using k and ϵ, with the help of the velocity and length scales as shown below [13]:

$$\mu_t = C\rho vl = \rho C_\mu \frac{k^{\frac{3}{2}}}{\epsilon} \tag{10}$$

where C is a dimensionless constant. The standard k-ϵ model, developed by Launder and Spalding, uses simplified transport equations and is included below [13] [14]:

$$\frac{\partial \rho k}{\partial t} + \nabla \cdot (\rho k \mathbf{U}) = \nabla \cdot [\frac{\mu_t}{\sigma_k} \nabla k] + \mu_t [\nabla \mathbf{U} + \nabla (\mathbf{U})^T] \nabla \mathbf{U} - \rho \epsilon \tag{11}$$

$$\frac{\partial \rho \epsilon}{\partial t} + \nabla \cdot (\rho \epsilon \mathbf{U}) = \nabla \cdot [\frac{\mu_t}{\sigma_\epsilon} \nabla \epsilon] + C_{1\epsilon} \frac{\epsilon}{k} \mu_t [\nabla \mathbf{U} + \nabla (\mathbf{U})^T] \nabla \mathbf{U} - C_{2\epsilon} \rho \frac{\epsilon^2}{k} \tag{12}$$

2.5.4 Wall Modelling

Wall models are used in order to model the near wall physics, allowing coarser meshes to be used in the near wall region, dependent on the turbulence model used. The level of refinement required for a mesh is dictated by the y+ value. When using the k-ϵ wall model, the ideal y+ value should range between 30 and 300, ideally aiming for 30 although this is not always possible. The immersed boundary method used in Foam-Extend-5.0 has its own set of k-ϵ wall models, for each variable [13].

2.5.5 Immersed Boundary Method

The immersed boundary method, developed by Peskin to evaluate blood flow through a heart, presents a viable methodology to solve moving body problems involving complex geometries [15]. The immersed boundary method has a number of different methodologies, including continuous forcing approaches, where the governing equations are edited pre-discretisation, and direct forcing, where the governing equations are edited post-discretisation. Within the Foam-Extend branch of OpenFoam, the intial implementation made use of a discrete forcing approach, namely the cut-cell method. In this method, the boundary of the geometry will cut through a Cartesian background cell. Depending on whether the cell centre is located in the geometry cells or the Cartesian cells will dictate if the cut cell becomes dead or if the cut cell is absorbed by surrounding Cartesian cells. In more recent Foam-Extend updates, a new method has been implemented, namely the immersed boundary surface method (IBSM) [13].

The IBSM works very similarly to the cut-cell approach previously discussed. An example of the IBSM has been included in Figure 1 [13]. The main difference is that in the cut-cell approach, it is only the cells whose cell centres are outside the geometry cells that are tagged as immersed boundary cells whereas within the IBSM, it is all cells that have been intersected by a boundary that are tagged as immersed boundary cells, irrespective of cell centre location. The other difference is that the cell that has been cut is not added into a cell, but instead becomes a cell of its own. This new cell will have a new cell centre, cell volume, face area and face centre that must be calculated, as well as a face area vector for the cut faces and new immersed boundary face. Any cells that are now dead are removed from the democratisation matrix, with new live cut cell data replacing the old cut cell data. This allows the immersed boundary to be added as a body fitted boundary condition on the fluid cells, allowing for the conventional FVM to be used, as described above [13] [16].

It must be ensured all cells are closed. For normal cells, the summation across all faces should be equal to zero, as shown in the equation below[13]:

$$\sum_C S_f = 0 \tag{13}$$

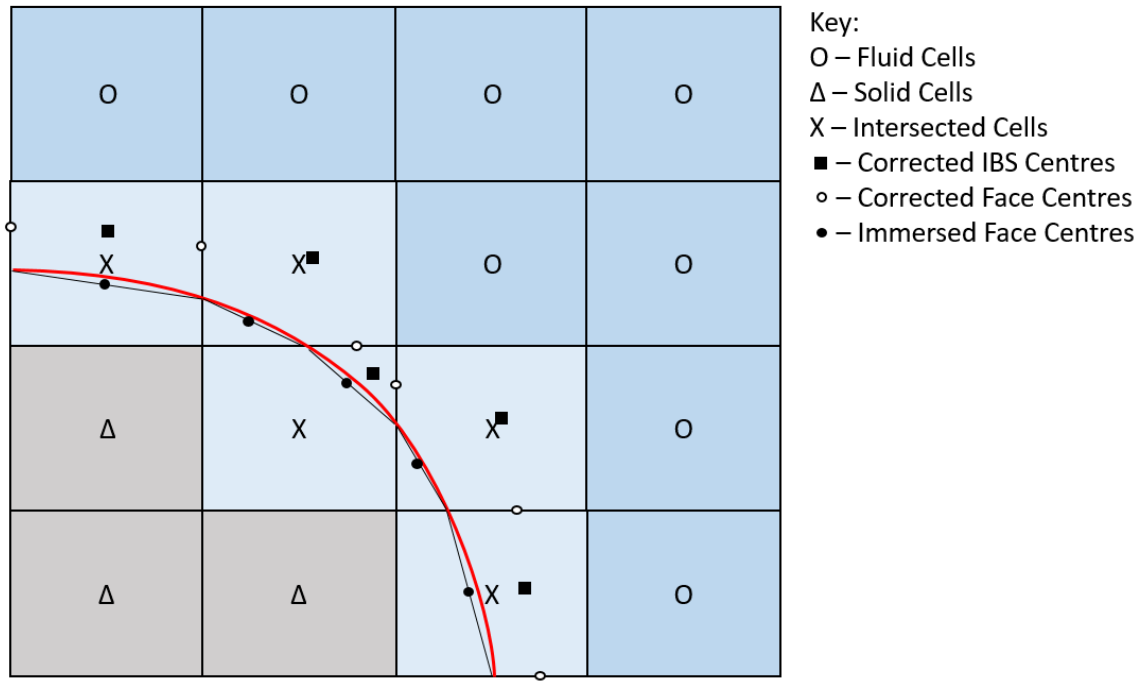

Figure 1: Passive drag geometry streamline position

A Marooney Manoeuvre is implemented for open cells, with old surface face area, S_f, corrected by a face correction. The corrected immersed boundary face area can then be added to the summation as shown below [13]:

$$S_{fIB} = -\underset{C}{\Sigma}\gamma_f S_f \tag{14}$$

2.5.6 Force Calculation

The final drag forces acting on the body are a combination of the normal pressure force and the tangential viscous forces as shown below [17]:

$$P_d = \underset{i}{\Sigma} S_f \rho_i S_f, i(P_i - P_{ref}) + S_{f,i} \cdot (\mu \mathbf{R}_{dev}) \tag{15}$$

where i is the identified cell, D is the passive drag, ρ is the density of the fluid, S_f is the face area vector, p is the pressure, μ is the dynamic viscosity, and $\mathbf{R}_{dev}$ is the deviatoric stress tensor.

3 Methodology

3.1 Active Drag Experiments

In order to validate CFD results, they must be compared to experimental results. The experimental set-up used in order to find the active drag of an athlete was similar to the set-up used by Haskins et al, and subsequently used by Cortesi et al [6] [18]. A thorough explanation of the experimental equipment and set-up is included in the referenced paper, with only the key information and changes included below.

As briefly described above, the method used by Haskins et al. made use of two separate experiments, including one fully tethered experiment using a load cell and one semi-tethered experiment using a 1080 Sprint resistance trainer (1080 Motion, AB, Lindingo, Sweden) [19]. The fully tethered equipment allows the propulsive force to be found across a stroke cycle, without the drag force acting as the athlete remains stationary in the water. The semi-tethered experiment allows the propulsive force to be found, including the drag force, as the athlete is moving through the water. The active drag can then be estimated by resampling the drag acting on a body swimming Freestyle across a stroke cycle for each case, to ensure consistent sampling points for both experimental conditions, and subtracting the semi-tethered data from the fully tethered data at each sampling point of the stroke cycle. This consistent sampling enables active drag changes across a stroke cycle to be compared across subjects, allowing averages and standard deviations to be calculated and plotted.

As the CFD simulations discussed later in this paper were single phase, both parts of the experiment (i.e. semi-tethered an fully-tethered trials) were completed with the swimmer completely submerged underwater, unlike the previous study in which all trials were conducted at the water surface. This allowed the single phase CFD to be compared with the experimental results. Ethical approval was granted for this study by the Engineering and Physical Sciences Research Ethics Committee at Queen's University Belfast. In this experiment, one Swim Ireland performance athlete was used, completing each part of the experiment twice. The athlete was instructed on each piece of equipment to hold his breath and swim at maximum effort underwater for as long as possible before surfacing and taking a breath. The athlete attempted to remain at an approximate water depth of 1 m, which ideally would have been with the aid of a guide rope, but due to pool set-up was not possible. Due to the non trivial nature of this experiment and athlete availability, the experiment could only be completed using one athlete. One final difference in the under water experiment relative to the previous surface-based study was that the athlete did not wear the SmartPaddles (Poolshark, Finland) force sensor equipment [20]. A diagram of the experiment has been included below in Figure 2:

A number of assumptions were made during the experiment:

- A consistent power output is assumed for each athlete during each part of the experiment, to allow the force values to be compared between different trials.
- A consistent technique is used by athletes during each part of the experiment, again to allow comparison between different trials.
- The 1080 Sprint and fully-tethered experiment will have limited impact on the overall technique of the athletes during the trials.
- It was assumed the stroke rate of the fully-tethered and semi-tethered experiment was constant for each trial.

The method used in order to resample, process the data, and identify stroke cycles was identical to that described in the previous study.

3.2 Unsteady Passive Drag Simulation Case

In order to investigate the reliability of the IBSM when applied to more complex geometry, simulations of a geometry in a passive drag position were completed. Passive drag in swimming is defined as the drag that acts around a body when in a fixed position, such as the glide position after a wall push or a diving start. The geometry for the passive drag cases was the same geometry that will be used for the active drag cases, developed by CodeThisLab [21]. There were some noted issues with the original geometry that required a redesign within the animation software Blender [22]. Some parts of the body, namely the shoulders, were prone to self intersection which could lead to errors in results. In order to address this, the geometry was put in the best streamline position possible whilst avoiding intersection. This geometry can be seen in Figure 3.

From this point the set-up was trivial. The cartesian mesh was set up using the blockMesh utility, followed by snappyHexMesh to refine the mesh around the geometry. Two regions were refined around

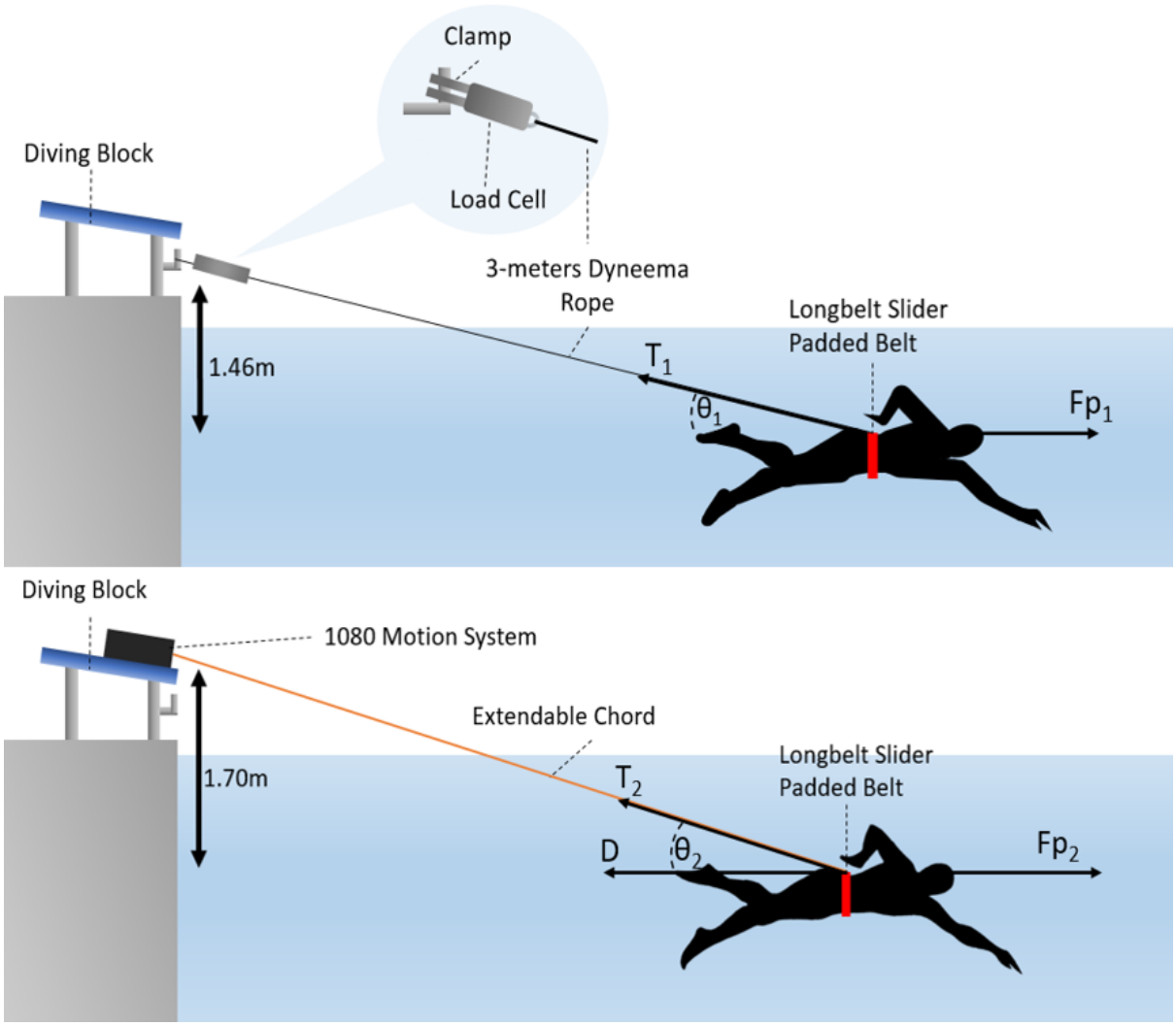

Figure 2: Underwater Active Drag Method

the body, an inner region and an outer region. A series of the refinement levels were investigated, namely a coarse, medium, and fine mesh. Due to the number of cells, a fourth further refined geometry was not possible, due to computational limitations of the available computing facilties.

After the mesh was generated, boundary conditions and initial conditions were applied. The inlet velocity was set at 2.00 ms^{-1}. IBSM wall models, designed for use with this method, were used for velocity, ϵ, p, and k. The cases were decomposed in order to allow for parallelisation of the problem, allowing the problem to be solved more quickly. In the set-up of numerical schemes, the time scheme was selected as Euler, with the gradient schemes set to linear, divergence schemes largely set to upwind, and the Laplacian scheme set to linear. Tolerances for k, ϵ, and U were set as $1x10^{-6}$ and the tolerance for p was set at $1x10^{8}$.

After decomposition, a potential flow initialiser is used, providing a more accurate initial condition for the simulations, improving subsequent convergence. After this, to further improve the chance of convergence in unsteady simulations, a simpleFoam case was run on the geometry for 1000 iterations. From this point the unsteady immersed boundary solver within OpenFOAM was used, namely pimpleDyMIbFoam.

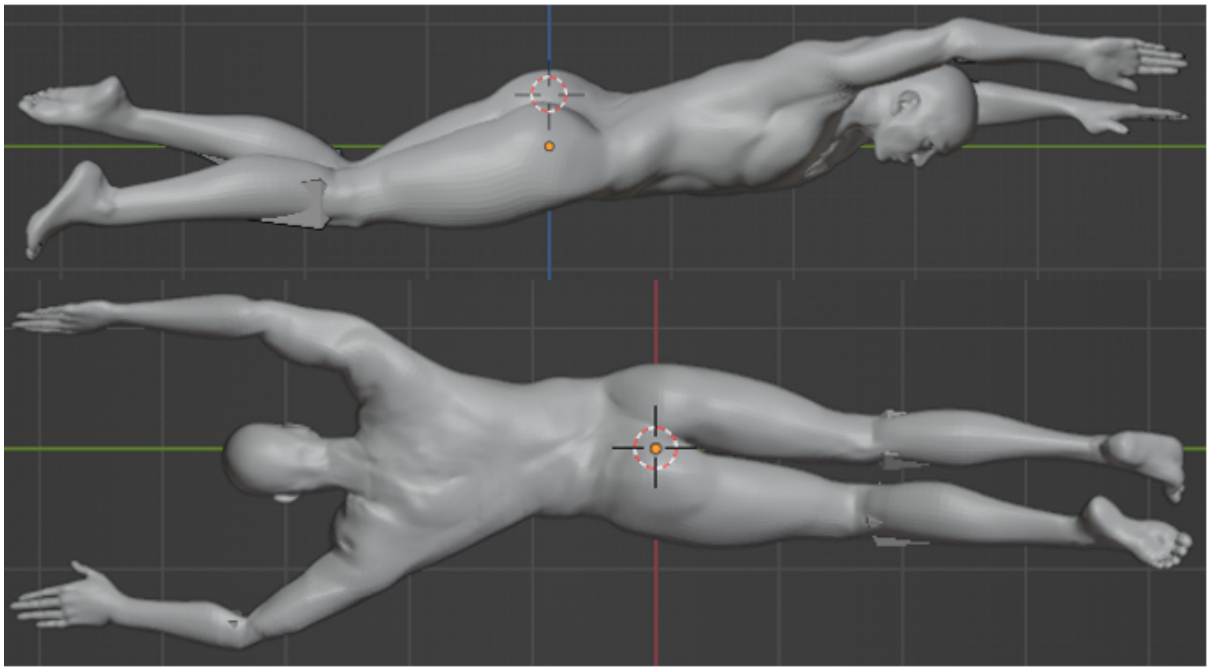

Figure 3: Passive drag geometry streamline position

Table 1: Cell counts used for each mesh refinement level

Mesh Refinement Level	Cell Count
Coarse	1,097,084
Medium	7,442,290
Fine	57,573,014

3.3 Quasi-Steady Active Drag Simulation Cases

Initially, it was hoped that active drag could be found using a novel add-on moving body immersed boundary surface method. Due to some simulation errors and time constraints it has not been possible to include results of this kind. A workaround to the moving body cases was developed, namely a quasi-steady approach. A quasi-steady approach is similar to a stop motion simulation, with the first position run as a typical simulation. The order of solver used on the first position was potentialFoam followed by simpleFoam and then pimpleDyMIbFoam. Following completion of the first simulation, the intial conditions of position 2 are set based on the final pimpleDyMIbFoam results of position 1. Position 3 initial conditions are set using only the final pimpleDyMIbFoam results from position 2 and the pattern repeats itself until all positions have undergone a pimpleDyMIbFoam simulation. This is shown by Figure 4.

In order to first test this method, some primitive geometry cases were run, namely 2D cylinders and 3D spheres. These cylinders and spheres were moved across a distance of 1 m in the x direction, with 101 keyframes describing the motion, i.e. 1 keyframe equal to moving 0.01 m. An image of the cylinder is included below in Figure 5

From this point the set-up was trivial. The cartesian mesh was set up using the blockMesh utility, followed by snappyHexMesh to refine the mesh around the geometry and around the area that the geometry will move into. A series of the refinement levels were investigated, a coarse, medium and fine mesh as displayed in 1. Due to the number of cells, a fourth further refined geometry was not possible, due to computational limitations.

The inlet velocity was set at 1.00ms. IBSM wall models, designed for use with this method, were used for velocity, ϵ, p and k. The cases were decomposed in order to allow for parallelisation of the problem, allowing the problem to be solved more quickly. In the set-up of numerical schemes, the time scheme

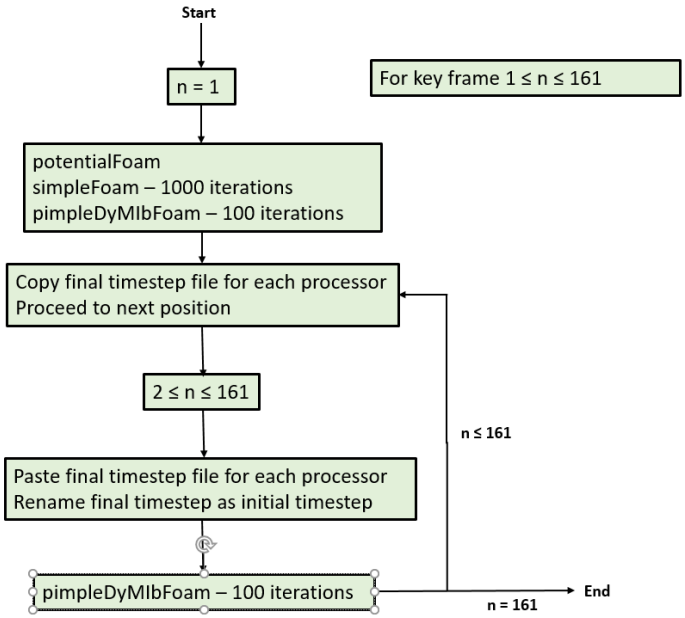

Figure 4: Work flow for quasi-steady approach

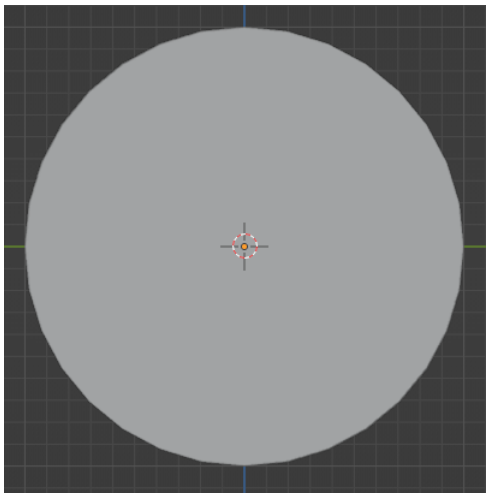

Figure 5: 2D Cylinder Geometry

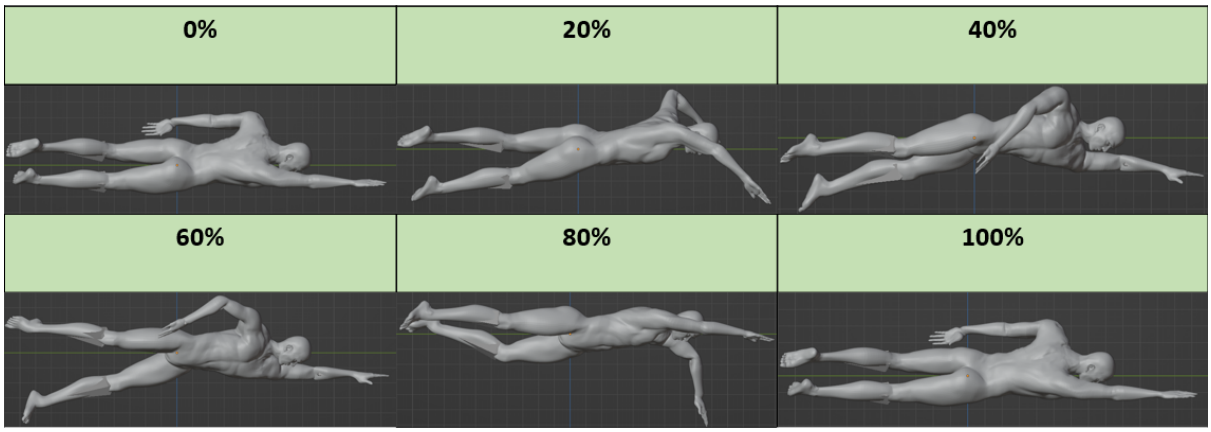

Figure 6: Standard Technique Key Positions

was selected as Euler, with the gradient schemes set to linear, divergence schemes largely set to upwind and the laplacian scheme set to linear. Tolerances for k, ϵ, and U were set as $1\text{x}10^{-6}$ and the tolerance for p was set at $1\text{x}10^{8}$.

After decomposition, a potential flow initialiser is used, providing a more accurate initial condition for the simulations, improving subsequent convergence. After this, to further improve the chance of convergence in unsteady simulations, a simpleFoam case was run on the geometry for 1000 iterations. From this point the unsteady immersed boundary solver within openFoam was used, namely pimpleDyMIbFoam. The timestep size was set at 0.001 with simulations allowed to run for 100 iterations. After 100 iterations, results for force had reasonably converged meaning further iterations were not required.

After the basic geometry cases, a very similar set-up was used in order to try and predict the active drag of a swimmer. In this case the same set-up was used except, instead of the keyframes used to depict the motion of a cylinder or sphere, 161 keyframes depicting a full freestyle stroke cycle were used to desribe the motion of the swimmer. A diagram of some of the key positions can be seen in Figure 6.

Beyond the geometry, the set-up was exactly the same with the exception that the inlet velocity was set to 2.00 ms^{-1}.

3.3.1 Varying Velocity

In reality, a swimmer's velocity varies during a full stroke. In order to run varying velocity simulations, more reflective of the changing values seen in real swimming, velocity data collected from the 1080 Sprint resistance trainer during the active drag experiment for a full Freestyle stroke cycle was resampled for the 161 timesteps used for the keyframes depicting the swimmer's motion (Figure 7). However, the quasi-steady approach employed for the constant velocity case was not directly applicable to a continuously varying velocity case.

In order to consider the variation of velocity, the inlet velocity must continue to change throughout each timestep. Since the quasi-steady approach solves each timestep as a constant velocity case, the final timestep of a given keyframe cannot be used as an initial value for the next keyframe. This means, in the varying velocity case, that time history effects from a previous position can not be included when applying the quasi-steady workflow described in Figure 4. A workaround to this issue was to simulate all variable velocity timesteps as independent cases, effectively ignoring the time history, by using the same protocol as the first timestep for *all* keyframes, i.e. running potentialFoam, simpleFoam, and then pimpleDyMIbFoam for *each* of the 161 positions (as opposed to just pimpleDyMIbFoam with the previous keyframe's final state as input for the second and later timesteps, as done in the constant velocity quasi-steady cases).

Before running a variable velocity case, a comparison of results between a quasi-steady case including time history between keyframes and the proposed workaround using independent simulations running

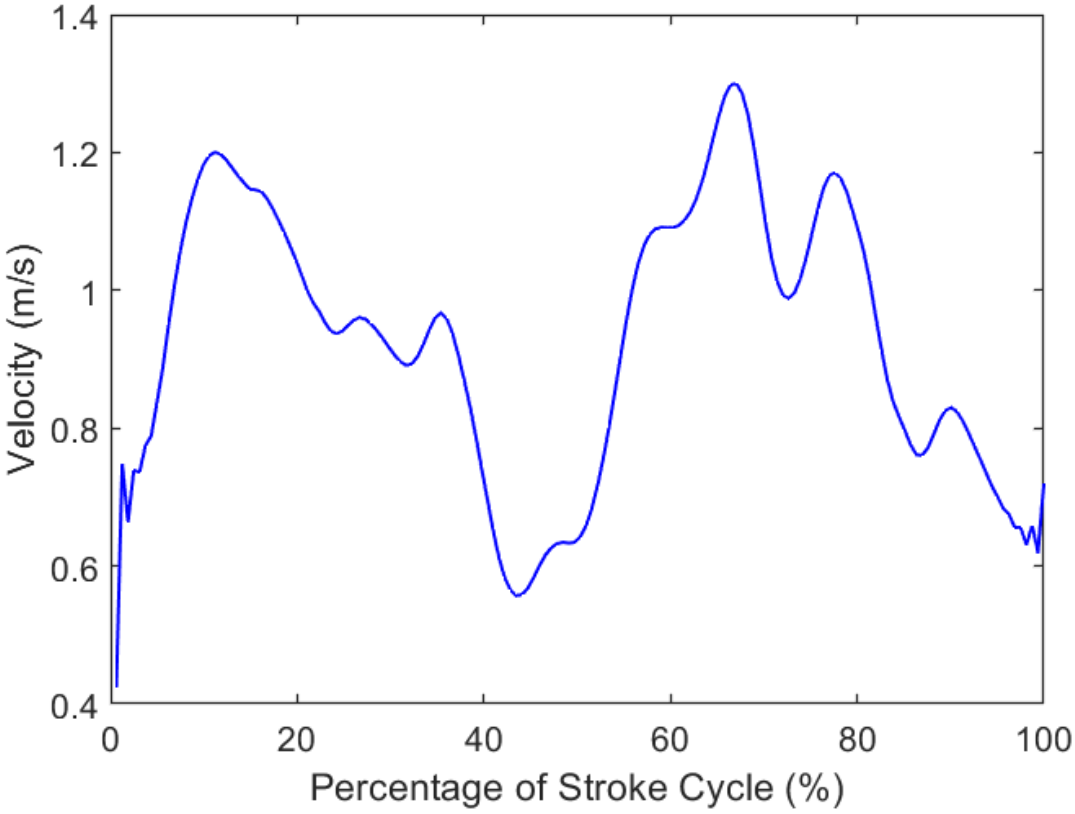

Figure 7: Velocity variation across a stroke cycle

potentialFoam, simpleFoam and pimpleDyMIbFoam method must be completed. This was achieved by comparing results of both approaches for a constant velocity case. This was completed at a velocity of 2.00 ms^{-1}, as this aligned more closely with studies from the literature and with the surface-based experimental results. The simulations will be rerun at 0.93 ms^{-1}, the average underwater velocity, in the near future.

Results show close alignment for both the trend and the values (Figure 8). The case where time history is considered has slightly higher values of drag, which is expected as it is likely that flow from the previous position will have an impact on the results in the current position. The difference in results appears to vary between positions, indicating some positions will have a greater impact than others on the drag at a future time. This could be down to the movement of flow around a geometry, implying that LES could be a valuable asset in understanding the differences in the flow patterns, due to its increased performance at resolving the large eddies in the flow. Importantly, as the results are not vastly different, results show that simulations that do not include time history, as proposed for the varying velocity workflow, can be useful first approximations of active drag.

One further limitation of both the quasi-steady and varying velocity cases is the absence of the inertial forces caused by the acceleration and deceleration of surrounding fluid.

3.4 Impact of Swimming Technique

One of the main considerations in this paper was to investigate the impact of changes in swimming technique on active drag profile. For reasons discussed in the results, investigating these technique changes was completed using the variable velocity approach outlined in Section 3.3.1. There were two main technique changes that were investigated, namely breathing and kick rate.

Starting with breathing, the standard animation used up to this point did not include the animation of

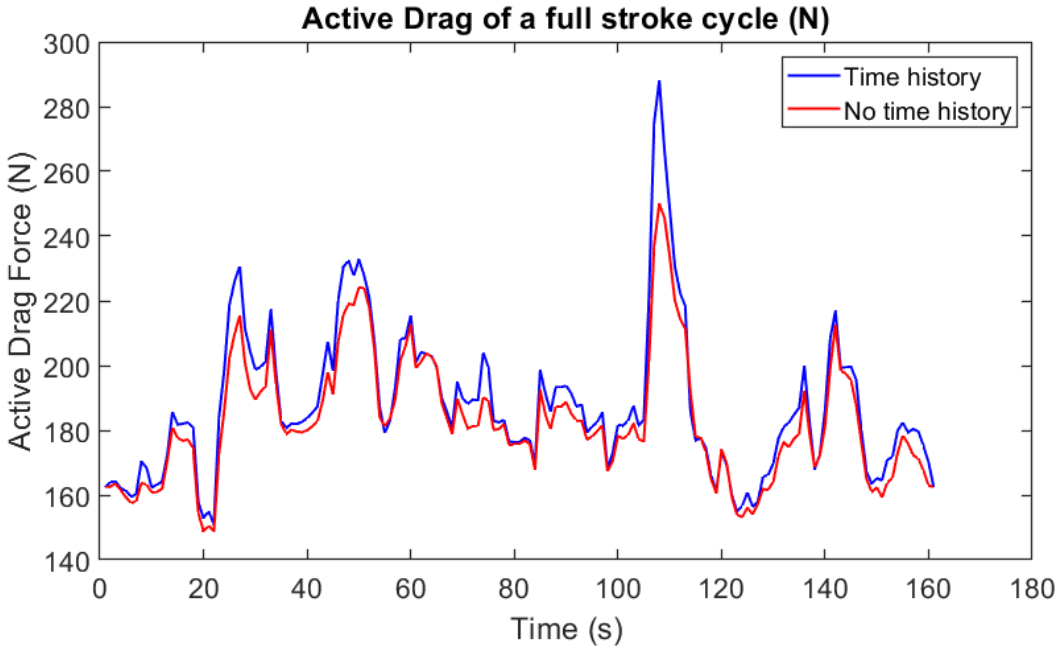

Figure 8: Quasi-steady time history vs no time history

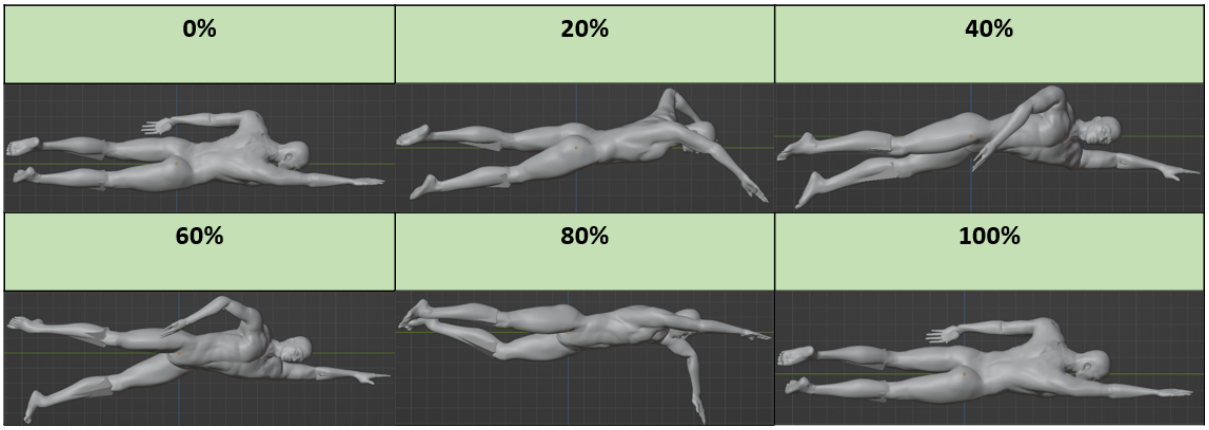

Figure 9: Key positions with swimmer taking breath.

a breath. As such, using Blender, an animation was created in which the swimmer takes a breath to his right side [22]. This is in line with the technical description given at the start of the paper. The second technique change involved changing the kick rate from a standard six-beat kick to a two-beat kick. Due to some issues in deforming the geometry, some minor simplifications to the motion were required to avoid self-intersections and excessive distortion in the mesh. Diagrams of these technique changes for some key positions are included below in Figure 9 and Figure 10 respectively.

4 Results and Discussion

4.1 Active Drag Experiment

Active drag forces were measured using the same method as Haskins et al. [6], as stated previously. The mean profile of the measured active drag force over a full stroke (Figure 11) appears reasonable, with two clear peaks and the magnitude of each of the peaks between 200-250 N. It is noted that there are some below-zero values of drag, possibly due to a limitation of the method. The profile of the active drag

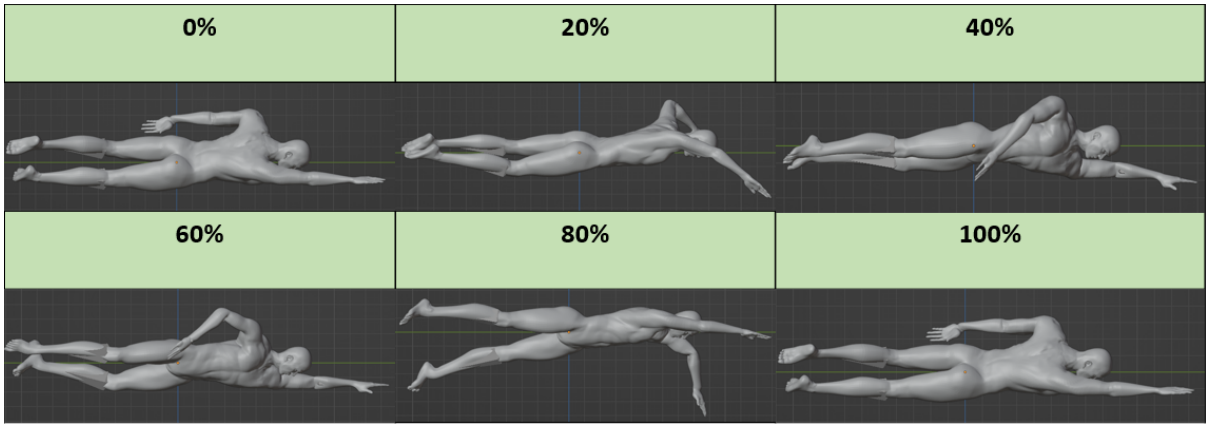

Figure 10: Key positions with two-beat kick.

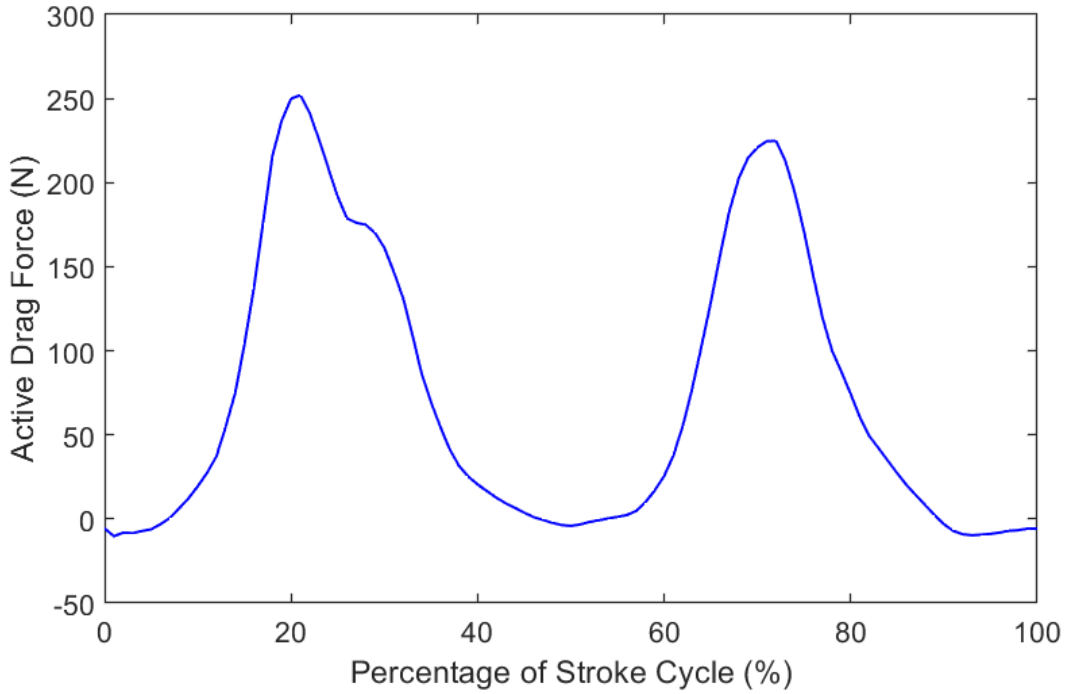

Figure 11: Underwater active drag results

Table 2: Pressure, friction, and total drag forces predicted by unsteady simulations for each mesh refinement level

Mesh Refinement Level	Pressure Drag Force (N)	Friction Drag Force (N)	Total Drag Force (N)
Coarse	153.2	10.9	164.1
Medium	117.7	14.3	132.0
Fine	104.1	16.4	120.5

force appears similar to the general profiles discussed by Haskins et al, with the peak forces marginally lower than those reported for surface-based swimming [6]. This is likely due to the difference in velocity caused by swimming solely underwater, which in this case was 0.93 ms^{-1}. In general, there is likely to be more drag experienced whilst swimming completely underwater than on the surface, provided the velocity of both trials was constant. Although there is no wave drag generated at a distance of between 0.6-0.8 m below the surface, the recovery of the arm through the fluid flow will increase the experienced drag substantially. The measured active drag also appears reasonable when compared to the ATM work of Formosa, with profiles appearing reasonably similarly, although Formosa certainly has more detailed fluctuations contained within the peaks [8]. Drag results collected by Formosa are again larger in the majority of cases, likely due to the velocities used, which appear to vary from approximately 1.7 to 1.9 ms^{-1} [8].

A number of limitations do exist within the experimental method. It can be difficult to exactly match the positions of each stroke between two different experiments, which is why it is suggested that a synchronised camera set-up could help minimise the errors introduced. Other limitations of this method will include the fact that asking a swimmer to attempt to swim with usual technique underwater is challenging, especially with regards to recovering the arms, and results will likely be impacted by this fact. The experiment was only completed on one athlete, meaning it is not possible to compare this profile to other similar profiles. This was simply due to athlete availability on the day and the challenging nature of what was being asked. Regardless of the challenges, the experiment did provide a result that can be used to compare to active drag CFD results.

4.2 Unsteady Passive Drag Simulations

The predicted drag forces for the unsteady passive drag simulations are included below in Table 2 and, although reasonable, do not appear to have reached a final state of convergence with respect to mesh refinement.

A thorough convergence study was completed using both a Grid Convergence Index (GCI) method and Richardson extrapolation [23]. The approximate order of the simulations is 1.46, which rounds down to the actual order of simulations being 1.00. Using a Richardson expansion, a value of 113.9 N was estimated for an infinitely small grid size. The percentage difference between the actual finest result and the perfect result is 5.45%, indicating results are reasonable. Finding a grid convergence index between the most coarse and medium mesh and the medium mesh and finest mesh results in values of 17.4% and 6.8% respectively [23], demonstrating that the simulations are converging with increasing refinement.

When compared to existing literature, passive drag results were over-predictive. Both Zaidi et al and Bixler et al estimated values of passive drag at 2 ms^{-1} to be approximately 55 N [24, 25]. Differences are likely caused by differences in position of the geometry: both Zaidi and Bixler had geometries in a position more reflective of a streamline position in swimming, with the arms tucked tighter by the head. This will likely have reduced the surface area and, as a result, the drag. In the geometry used for the current study, the less tight streamline will result in a higher surface area and hence a higher value of passive drag. When compared to a more similar position, namely the work of Zahn [26], results are significantly closer, with Zahn reporting a passive drag value of approximately 115 N. This suggests that simulations are reasonably accurate for complex shapes, provided overall pose is approximated well. These results, in combination with the mesh refinement study, demonstrate that the immersed boundary surface method can be applied to complex shapes successfully.

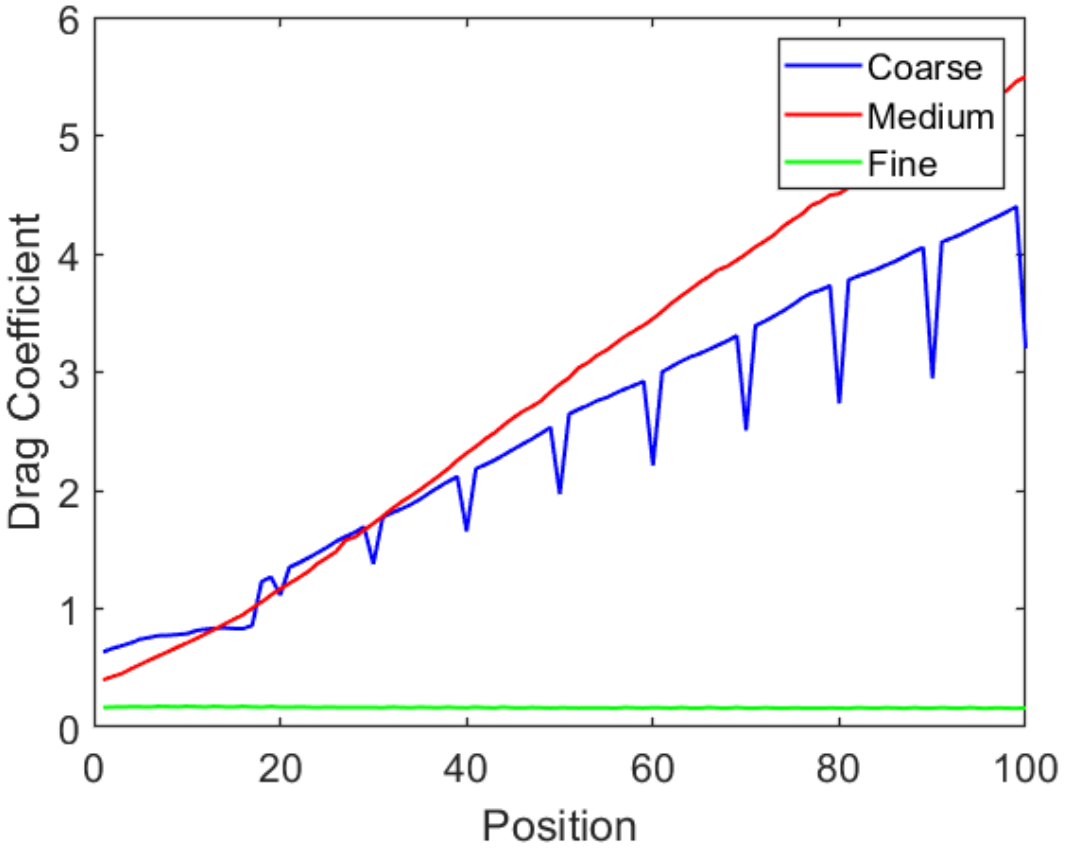

Figure 12: Predicted drag coefficient for cylinder translating underwater.

4.3 Quasi-steady Simulations

4.3.1 2D Translating Cylinder

Predictions for drag coefficient of a 2D translating cylinder (Figure 12) are under-predictive when compared to existing literature: predicted drag coefficient for the fine case was approx. 0.18 and whereas the expected drag coefficient was approx. 1.10 [27]. There is clearly some form of divergence occurring with the coase and medium mesh cases that will need further investigation. Based on previous work, when predicting results around a 2D bluff body, the k-omega method has been shown to provide better results and as such, may be worth investigating. The k-ϵ model was used in these validation simulations as this was the turbulence model that would be used in the active drag simulations, due to the coarser grid requirements.

4.3.2 Active Drag during Underwater Swimming

The quasi-steady simulations predicted active drag for the full stroke cycle for both coarse and medium mesh refinement levels (Figure 13), although some difficulties were noted. When the first coarse simulation was run, results appeared to fluctuate quite heavily, although there were some stand-out peaks that appeared to be of a similar magnitude to the experimental measurements. However, beyond the result magnitude, there were no further similarities in the shape of the quasi steady results and the experimental results. Initially, it was thought to be a refinement issue, with the Cartesian grid thought to be too coarse to pick up the details of the swimmer geometry, meaning results were not being calculated accurately around each detail of the geometry.

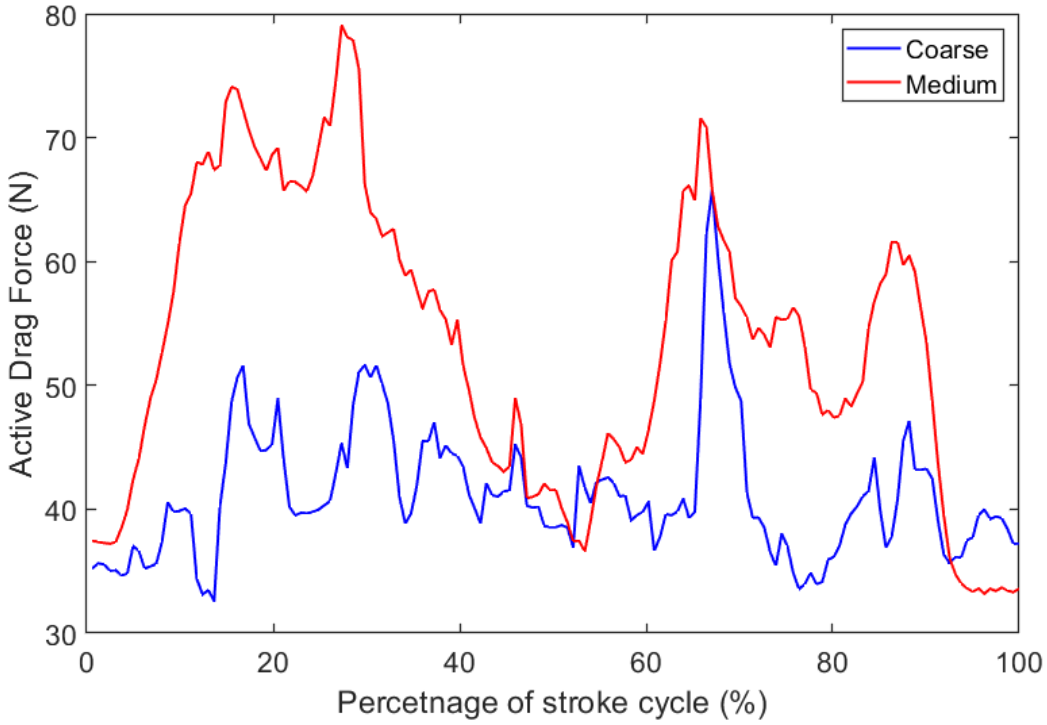

Figure 13: Quasi-steady predictions of active drag force during underwater swimming for coarse and medium meshes.

Upon trying to run a medium level mesh case, results were almost unusable, with a number of key frames diverging and predicted magnitudes far greater than expected. It was thought that the mesh geometry itself was likely the issue as the simulations were first order, which should be stable, and had worked well for a complex passive drag case. It is possible that the cells on the geometry were resulting in the formation of highly skewed immersed boundary cells that would impact how variables were projected onto the cell faces, potentially leading to divergence. As such, the geometry was imported to MeshLab and each position was both coarsened and refined to visualise the impact on the results [28]. The simulation was repeated using the coarser swimming geometry, failing almost immediately, and the more refined swimming geometry, working better on the medium background mesh.

Results for the medium quasi-steady approach were more reasonable when compared to the active drag experimental results than those for the constant velocity simulations (which did not capture the two main peaks within the stroke — compare predicted force for a constant velocity in Figure 8 to the measured forces in Figure 11), demonstrating the importance of incorporating the subject-specific velocity profile within the simulation. Results for the coarse case were unchanged, likely due to the same Cartesian mesh being used with some geometry details again ignored. Results clearly show some general trends for the medium cases that are present in the underwater experimental method. Certainly it can be seen there are trends that resemble the identifiable peaks, although more peaks are present in the computational cases when compared to the experimental cases. It is noted that computationally predicted magnitudes of active drag were larger compared to the experimental results, likely due to the fact the CFD was run at a fixed velocity of 2 ms^{-1} for all positions, whereas average experimental velocity was 0.93 ms^{-1}.

When the Cartesian mesh was refined to a fine mesh, simulations appeared to fail for the same reasons as stated when moving from a coarse to medium mesh with the original geometry. Results appeared to diverge across a large number of positions and further refining the geometry to fix this would have resulted in too many cells on the geometry, which could lead to further issues like Blender crashing or ParaView hanging [29]. A possible workaround is to reposition some problem positions to try and reduced the risk of failure by avoiding sharp angles, overlapping geometry, and tight corners. This workaround is incredibly time consuming and requires constant observation. These non ideal geometry issues are likely due to the fact that the original model is developed for animation and not research, meaning there is

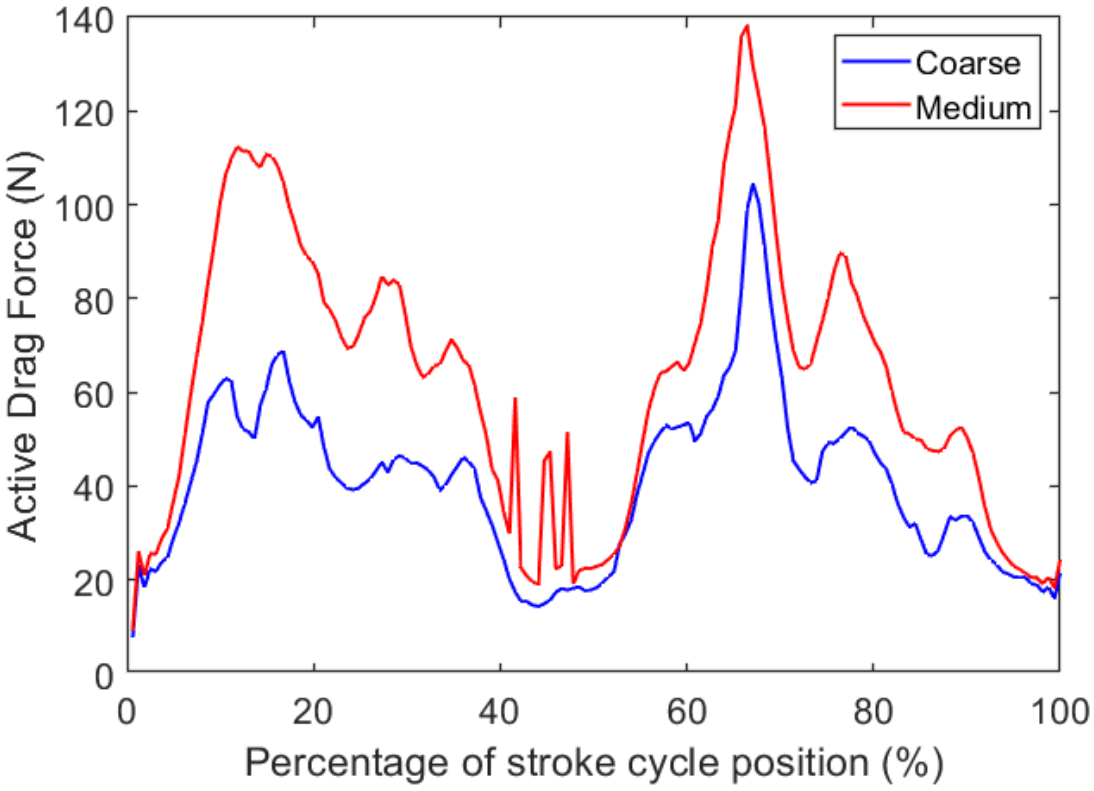

Figure 14: Varying velocity coarse and medium mesh

possibly excessive detail in the model that can lead to the aforementioned issues. Other solutions would be to reanimate a new geometry more accurately with less surface detail, although from experience, there is a fine balance between ease of animation and detail required to animate. As model detail decreases, it becomes increasingly difficult to successfully animate realistic motions.

An alternative method to address these complex issues may be to use a different version of the immersed boundary method. A continuous forcing approach applies the immersed boundary as an additional term in the momentum equations, before discretisation. A force acting on the immersed boundary can be multiplied by the Dirac delta function, which is equal to 1 at an immersed boundary [13]. The Lagrangian immersed boundary usually does not align with the Eulerian background mesh, meaning the sharp impulse function is then applied to the boundary and the neighbouring cells, helping to smooth the distribution. Although this is mainly for elastic boundaries, lower Reynolds number rigid body extensions exist. Significant amounts of further investigation would be required however [13].

Based on the reasoning of the time history compared to the no time history case, the varying velocity simulation approach, as described in Section 3.3.1, was applied to the same coarse and medium meshes as used for the unsteady case to predict the active drag force for the varying velocity profile measured in the active drag experiment (Figure 14). The general shape of Figure 14 is similar to Figure 11 in that there are two identifiable main peaks for both coarse and medium refinements, although the CFD results contain numerous additional oscillations. The general magnitude of the active drag forces across the stroke cycle are also more appropriate when varying velocity is included compared to the underwater active drag measurements, although are still under-predictive. Reasons for the difference in drag force may be due to the inertial forces arising from added mass of accelerating and decelerating regions of fluid being ignored. This will have a substantial impact on not only the profile but the magnitude of active drag, especially for a single-phase submerged swimmer simulation.

Results also differ from the work of Formosa et al [8] and Haskins et al [6], as the experimental measurements in those studies were completed on the surface. Nevertheless, common themes have been identified in the general trend when compared to both of those studies. Finally, as noted already, there are more

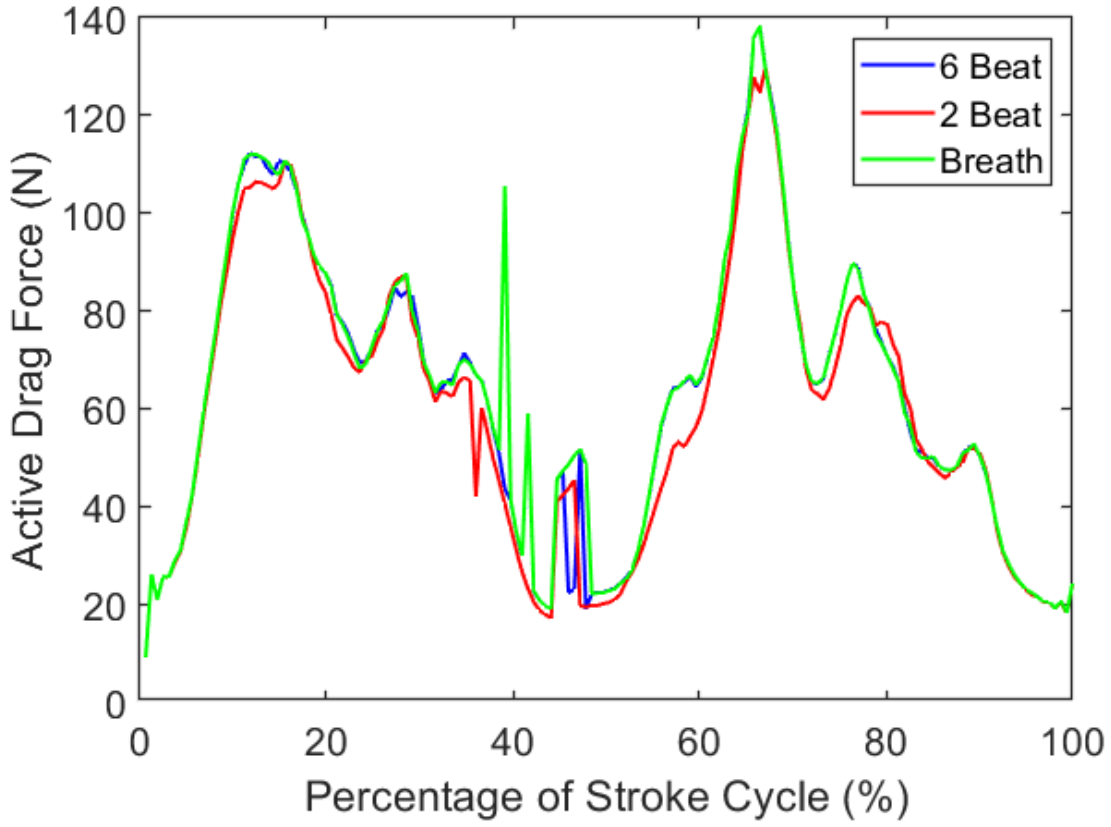

Figure 15: Active drag with technique changes

fluctuations in the CFD predictions than in the underwater active drag experimental measurements, likely due to the sudden change in position, but this would need further investigation.

4.3.3 Impact of Technique Changes

The change in technique was investigated using a medium grid refinement, as a fine grid simulation was not successfully run. The results of the changing technique are included in Figure 15. Results appear reasonable in terms of magnitude, although they are again relatively low compared with the experimental measurements, which may be caused by not solving for the inertial forces. It is also evident that there is not much difference in the results between each technique change. There is some difference between the forces of the different kick rates, although it is mostly small, apart from a few specific regions (e.g. at approximately 60% of the stroke). This could indicate that changing the kick rate is a relatively minor technical change, assuming the kick strength remains constant, that results in very little change in drag. Apart from some changes in the peaks between 40–50% of the stroke, breathing did not noticeably affect the predicted drag. The breathing position sees very little change to the technique beyond a slight head tilt, so it may make sense that the profile is almost identical to the 6 beat kick with no breath.

There could be a number of reasons for the similar profiles, including the fact that the mesh is not particularly fine and, as a result of this, each technique change may not be accounted for accurately by the mesh size. Further to this, accounting for the drag caused by recovering the arm under the water could cause over-prediction for large parts of the the profile which could overwhelm differences due to the technique changes. As noted already, there are some increased fluctuations in each result, especially in the breathing result, likely indicative of the geometry issues interacting with the Cartesian mesh refinement level discussed earlier.

5 Conclusion and Future Work

5.1 Conclusions

The immersed boundary surface method in Foam-Extend was demonstrated as a promising method to explore active drag forces during swimming. While there were issues with robustness of the immersed boundary surface method with respect to the quality and refinement of the body mesh, as well as the background Cartesian mesh, the approach was demonstrated to be capable of handling very complex geometries. It is possible that some different immersed boundary methods, such as a continuous forcing approach, could provide reasonable results, although this would need further investigation. Beyond this, there are a number of conclusions that can be drawn from each section of the work as follows:

5.1.1 Active Drag Experiment Conclusions

The active drag underwater experiment allowed for further validation of the methodology. The general trend in measured drag forces was similar to both literature and previous surface-based experiments conducted by the authors, although there were some evident differences caused by swimming solely underwater. It is recommended this active drag methodology be completed on the surface, as completed in the original publication [6]. It is also recommended that more than one swimmer should be used during this experiment for future comparison of single-phase active drag cases.

5.1.2 Passive Drag Simulation Conclusions

Predictions of passive drag force during underwater towing followed similar trends compared to the appropriate literature and measured forces during underwater towing, implying that the immersed boundary method is a useful tool for predicting drag around complex shapes. The mesh refinement study highlighted the importance of determining appropriate refinement levels for both moving body and background fluid meshes. It is therefore recommended that, when using the immersed boundary method, some significant time must be given to obtaining an accurate and robust geometry, allowing for further improvements in predicted drag results.

5.1.3 Quasi-steady Simulation Conclusions

Predictions for drag coefficient acting around a cylinder are mixed, with only the fine case being reasonable. It is likely that there have been some errors introduced in the results, potentially due to case set-up, that will need further investigation.

A key finding from the quasi-steady simulations of active drag was that incorporating the subject-specific velocity profile from the experiment was essential when trying to match the general profile of active drag force during a full stroke. However, this required the quasi-steady solution procedure to be modified (by treating each timestep as an independent analysis, effectively ignoring the simulation's time history) as it was not possible to use the converged results from a different fluid velocity in a prior step as the initial condition for a given fluid velocity of the next step. Fortunately, based on the time history comparison test, it was shown that neglecting time history is viable in order to consider a varying velocity case. Issues with the relative refinement between the moving body mesh and background fluid mesh indicate again that some significant time must be given to obtaining an accurate geometry, allowing for further improvements in predicted drag forces. Improvements to the geometry would also likely allow for finer background mesh analysis, as would be required for a grid convergence study. It is also recommended to make an attempt in accounting for the added mass impact experienced during these simulations, which would likely improve the accuracy of results. Results do however show that the IBSM is a useful method in predicting drag forces.

5.1.4 Technique Change Simulation Conclusions

The differences in drag profile appear minimal when considering various technique changes in freestyle swimming. There are some small differences existing when comparing 2 beat and 6 beat kick, potentially as the body position is being impacted more than when breathing, although this would need further investigation. It is recommended that a finer mesh and grid convergence study are completed, with changes in profile likely more visible using a finer background mesh. Again, it is recommended that some significant time must be given to obtaining an accurate geometry, allowing for further improvements in predicted drag forces.

5.2 Future Work

In the future one of the main aims would be to address the immediate geometry concerns, hopefully allowing for more robust moving body solutions to the simulations. One such method could be combining 3D scanning of a swimmer's geometry with measured 3D kinematic data of the same person to make a more realistically animated swimming model. Further work could involve integrating an overset mesh within the immersed boundary method, allowing for further mesh size reduction. This could be quite complex, due to the complex 3D motions, especially around the arms. One final piece of further work would involve incorporating the multi-phase aspect of these simulations, as a necessity to improve the active drag results for surface-based swimming. With these problems addressed, results could be more robust and realistic, allowing for investigation of other swimming disciplines, namely Backstroke, Breaststroke, and Butterfly. This would allow further investigation of the viability of the immersed boundary surface method as a useful and robust CFD tool for complex problems.

References

[1] Rumyanstev V. A. Voronstov, A. R. Resistive forces in swimming, biomechanics in sport.

[2] Carl Payton, Luke Hogarth, Brendan Burkett, Peter Van De Vliet, Sandra Lewis, and Yim Taek Oh. Active drag as a criterion for evidence-based classification in para swimming. *Medicine and Science in Sports and Exercise*, 52:1576–1584, 7 2020.

[3] Stan Shepherd. Personal discussion, lisburn city swimming club head coach.

[4] A. P. Hollander et al. Measurement of active drag during crawl arm stroke swimming, 1986.

[5] Angus Webb, Joseph Banks, Christopher Phillips, Dominic Hudson, Dominic Taunton, and Stephen Turnock. Prediction of passive and active drag in swimming. volume 13, pages 133–140. Elsevier Ltd, 2011.

[6] A. Haskins, C. McCabe, R. Kennedy, R. McWade, A. B. Lennon, and D. Chandar. A novel method of determining the active drag profile in swimming via data manipulation of multiple tension force collection methods. *Scientific Reports*, 13, 12 2023.

[7] Bruce Mason, Gina Sacilotto, and Tracey Menzies. Estimation of active drag using an assisted tow of higher than max swim velocitythat allows fluctuating velocity varying tow force.

[8] D. Formosa, M. G.L. Sayers, and B. Burkett. The influence of the breathing action on net drag force production in front crawl swimming. *International Journal of Sports Medicine*, 35:1124–1129, 6 2014.

[9] Matt Keys BEng. Establishing computational fluid dynamics models for swimming technique assessment, 2010.

[10] Alfred Von Loebbecke, Rajat Mittal, Frank Fish, and Russell Mark. Propulsive efficiency of the underwater dolphin kick in humans. *Journal of Biomechanical Engineering*, 131, 5 2009.

[11] Raymond C.Z. Cohen, Paul W. Cleary, Bruce R. Mason, and David L. Pease. Studying the effects of asymmetry on freestyle swimming using smoothed particle hydrodynamics. *Computer Methods in Biomechanics and Biomedical Engineering*, 23:271–284, 5 2020.

[12] Foam-Extend-5.0.

[13] Jan Erik Döhler. An analysis of the immersed boundary surface method in foam-extend.

[14] D.B. Spalding B.E. Launder. The numerical computation of turbulent flows. *Computer Methods in Applied Mechanics and Engineering*.

[15] C. S. Peskin. Flow patterns around heart valves: A numerical method. *Journal of Computational Physics*.
[16] Hrvoje Jasak. Immersed boundary surface method in foam-extend.
[17] User guide V2112 OpenFoam (2016) Forces. *OpenFoam (2016) Forces*.
[18] Matteo Cortesi, Giorgio Gatta, Rémi Carmigniani, and Paola Zamparo. Estimating active drag based on full and semi-tethered swimming tests. *Journal of Sports Science and Medicine*, 23:17–24, 3 2024.
[19] 1080 Motion. *Https://1080motion.Com*.
[20] SmartPaddle. *https://trainesense-shop.myshopify.com/*.
[21] CodeThisLab. *Male Animated Swimmer HQ 001 3D. Shutterstock*.
[22] Tom Roosendale. Blender.
[23] P J Roache. Quantification of uncertainty in computational fluid dynamics, 1997.
[24] H. Zaïdi, S. Fohanno, R. Taïar, and G. Polidori. Turbulence model choice for the calculation of drag forces when using the cfd method. *Journal of Biomechanics*, 43:405–411, 2 2010.
[25] Barry Bixler, David Pease, and Fiona Fairhurst. The accuracy of computational fluid dynamics analysis of the passive drag of a male swimmer. *Sports Biomechanics*, 6:81–98, 2007.
[26] Jie Min Zhan, Tian Zeng Li, Xue Bin Chen, Yok Sheung Li, and Wing Hong Onyx Wai. 3d numerical simulation analysis of passive drag near free surface in swimming. *China Ocean Engineering*, 29:265–273, 4 2015.
[27] R. Panton. Incompressible flow. 4th edition.
[28] ISTI CNR. https://www.meshlab.net/.
[29] Los Alamos National Laboratory Kitware, Sandia National Laboratories. https://www.paraview.org/.

6 Acknowledgements, Funding and Contributions

6.1 Acknowledgements

The authors would like to thank Stan Shepherd as well as the Swim Ireland coaches and athletes for their contribution to the study, especially for the lane space. The authors would also like to thank Ulster University for their expertise and support throughout the study in collecting the experimental results.

6.2 Funding

The authors would like to thank and acknowledge funding from the Department for the Economy that made this study possible

6.3 Contributions

A.H. planned and developed the study concept including the experimental work, geometry validation, passive and active drag simulations with thorough input from A.L. and D.C. C.M. and R.K. aided in the collection of the active drag data, with C.M. involved in developing the original experimental method. A.H. performed the simulations and post processing of all data, with assistance provided from A.L. and D.C. D.C. generated the and compiled the Foam-Extend code that allowed this study to be possible, as well as writing the moving body solver. A.H. wrote the first draft with alterations advised by A.L. and D.C. A.H. completed the revisions.

6.4 Competing Interests

The authors declare no competing interests

6.5 Corresponding Author

Correspondence to Alex Lennon